



**HAL**  
open science

## Spectral induced polarization of partially saturated clay-rocks: a mechanistic approach

D. Jougnot, A. Ghorbani, A. Revil, Philippe Leroy, P. Cosenza

► **To cite this version:**

D. Jougnot, A. Ghorbani, A. Revil, Philippe Leroy, P. Cosenza. Spectral induced polarization of partially saturated clay-rocks: a mechanistic approach. *Geophysical Journal International*, 2010, 180, pp.210-224. 10.1111/J.1365-246X.2009.04426.X . insu-00548746

**HAL Id: insu-00548746**

**<https://insu.hal.science/insu-00548746>**

Submitted on 8 Mar 2021

**HAL** is a multi-disciplinary open access archive for the deposit and dissemination of scientific research documents, whether they are published or not. The documents may come from teaching and research institutions in France or abroad, or from public or private research centers.

L'archive ouverte pluridisciplinaire **HAL**, est destinée au dépôt et à la diffusion de documents scientifiques de niveau recherche, publiés ou non, émanant des établissements d'enseignement et de recherche français ou étrangers, des laboratoires publics ou privés.

# Spectral induced polarization of partially saturated clay-rocks: a mechanistic approach

D. Jougnot,<sup>1,2,3</sup> A. Ghorbani,<sup>4</sup> A. Revil,<sup>2,3</sup> P. Leroy<sup>5</sup> and P. Cosenza<sup>6</sup>

<sup>1</sup>ANDRA, 1-7 rue Jean Monnet, 92298 Châtenay-Malabry, France. Email: arevil@mines.edu

<sup>2</sup>CNRS-UMR 5559-LGIT, Université de Savoie, Equipe volcan, 73376 Le-Bourget-du-Lac, France

<sup>3</sup>Colorado School of Mines, Department of Geophysics, Golden, 80401, CO, USA

<sup>4</sup>Department of Mining and Metallurgy, Yazd University, Yazd, Iran

<sup>5</sup>BRGM, 3 avenue C. Guillemin, BP 36009, 45060 Orléans, France

<sup>6</sup>FRE CNRS 3114 HydrASA, Université de Poitiers, France

Accepted 2009 October 20. Received 2009 October 19; in original form 2009 August 22

## SUMMARY

We have developed a mechanistic model to interpret spectral induced polarization data of partially saturated clay-rocks. This model accounts for the polarization of the grains through an electrical double layer model with a polarization model of the inner part of the electrical double layer called the Stern layer. The polarization model accounts also for the Maxwell–Wagner polarization at frequencies higher than 100 Hz. The Maxwell–Wagner polarization is modelled by using a conductivity model modified to account for the presence of a non-wetting immiscible phase like air in the pore space. The resulting model is consistent with the first and second Archie's laws in the case where surface conductivity can be neglected. The volumetric charge density of the diffuse layer at saturation is divided by the saturation of the water phase to account for the partial water saturation of the porous material. The model comprises seven fundamental parameters: the formation factor, the second Archie's exponent, a critical water saturation level, the mean electrical potential of the pore space at saturation, the density of the counterions in the Stern layer, and at least two parameters describing the grain size distribution. Most of these parameters can be derived independently using alternative measurements and electrochemical models. Measurements were performed in the frequency range 10 mHz–45 kHz using five samples from the Callovo–Oxfordian formation in the eastern part of the Paris Basin, France. The model agrees fairly well with the experimental data at saturation and for partially saturated clay-rocks down to 1 Hz. Most of the seven physical parameters entering the model were independently evaluated.

**Key words:** Electrical properties; Electromagnetic theory; Hydrogeophysics; Permeability and porosity.

## 1 INTRODUCTION

Spectral induced polarization reports the modulus of the conductivity and the phase between the current and the voltage in the frequency domain (typically from few millihertz to few tens of kilohertz, sometimes few Megahertz). The modulus and the phase can also be recasted into an equivalent complex conductivity or complex resistivity. This method has been developed first to locate ore bodies (Marshall & Madden 1959; Van Voorhis *et al.* 1973) and more recently in environmental sciences (Kemna *et al.* 2000, 2004; Slater & Binley 2006; Hördt *et al.* 2007; Blaschek *et al.* 2008). In environmental sciences, spectral induced polarization has been used to map contaminants in the ground (Vanhala 1997b), to determine grain size distribution (Lesmes & Morgan 2001; Leroy *et al.* 2008) and permeability (Börner *et al.* 1996; de Lima & Niwas 2000; Binley *et al.* 2005; Hördt *et al.* 2007). In parallel to these new types

of investigations, the improvement of high accuracy acquisition systems able to measure the phase with a precision of 1–0.1 mrad (Zimmermann *et al.* 2008) has allowed to investigate rock samples and soils characterized by very low quadrature conductivity including glass beads (Leroy *et al.* 2008), clean (clay-free), sandstones (Binley *et al.* 2005) and clay materials (Ghorbani *et al.* 2009).

During the last few years, several works have been done in using spectral induced polarization to study the properties of clay-rocks (Kruschwitz & Yaramanci 2004; Cosenza *et al.* 2008; Tabbagh *et al.* 2009). These works were motivated by the use of the spectral induced polarization method to study nuclear waste disposals (Kruschwitz & Yaramanci 2004; Pusch 2006) and generally speaking to study the role of clay barriers for the confinement of different types of hazardous materials. Indeed, because of their high-specific surface area and very low permeabilities ( $<10^{-19}$  m<sup>2</sup>) (Gaucher *et al.* 2004), clay-rocks are good candidates for host rocks (Homand

*et al.* 2004). Various national agencies (like ANDRA in France) have been commissioned to study the transport properties, speciation and thermohydro-mechanical behaviour of clay-rocks. These works will allow to assess the long-term safety of future potential radioactive waste disposals in these materials.

In order to study these clay-rocks formations, underground research laboratories have been built like Bure in France and Mol in Belgium or test sites have been selected, like Tournemire in France, and Mont Terry in Switzerland. Gallery excavations in these laboratories have generated perturbations of the rock: the Excavated Damaged Zone (EDZ) along the walls of the galleries (Tsang *et al.* 2005). To improve the knowledge of these zones, geophysical methods can provide very useful information especially spectral induced polarization as shown by Kruschwitz & Yaramanci (2004). Additional investigations were performed in the laboratory, which confirm this possibility (Cosenza *et al.* 2007; Ghorbani *et al.* 2009). However, all these authors used semi-empirical approaches based on the Cole–Cole model (Cole & Cole 1941; Ghorbani *et al.* 2007; Chen *et al.* 2008) or similar semi-empirical models like the Davidson–Cole model (Davidson & Cole 1950) and the generalized Cole–Cole model (Vanhalo 1997a; Ghorbani *et al.* 2009). Leroy & Revil (2009) have proposed recently a mechanistic model to quantify spectral induced polarization in saturated clay-rich materials. However, a quantitative understanding of spectral induced polarization data in unsaturated clay-rocks is still missing.

We propose below a mechanistic model of spectral induced polarization of unsaturated clays-rocks. This model is based on an extension of the theory developed recently by Leroy & Revil (2009) for clay-rich materials. This model extends also some previous modelling efforts to understand cross-coupling properties of clay

materials (Revil & Leroy 2004; Revil & Linde 2006). We also compare the prediction of this new model to new spectral induced polarization measurements performed on five core samples from the Callovo–Oxfordian clay-rock formation. This formation is presently studied by ANDRA, the French Nuclear Waste Agency, as a potential host for nuclear wastes.

## 2 DESCRIPTION OF THE CALLOVO–OXFORDIAN CLAY-ROCK

ANDRA has developed an underground research facility, the test site of Bure, to study the possibility of long-term underground disposal of nuclear wastes. The site of Bure (Meuse/Haute-Marne, France) is located in the eastern part of the Paris Basin in a thick clay-stone formation of Callovian to Oxfordian age (Fig. 1). At Bure, the Callovo–Oxfordian formation has a thickness of approximately 130–160 m. The Callovo–Oxfordian formation can be subdivided in four main lithofacies units. At Borehole EST205 (see location in Fig. 1), we find first the C2d unit for depths comprised between approximately 417 and 437 m. This unit presents some smooth spatial variations in the mineralogy and petrophysical properties. The C2c and C2b units are located between approximately 437 and 456 m. These units are relatively homogeneous. The bottom unit C2b of the Callovo–Oxfordian formation unit is itself divided into two subunits: C2b2 (approximately 456–473 m) and C2b1 (approximately 473–508 m). The subunit C2b1 corresponds to the unit where the proportion of clay minerals is the highest through the Callovo–Oxfordian formation and is located at depths comprised between approximately 486 and 489 m. The underground laboratory of ANDRA at Bure is located just below this level. The bottom unit

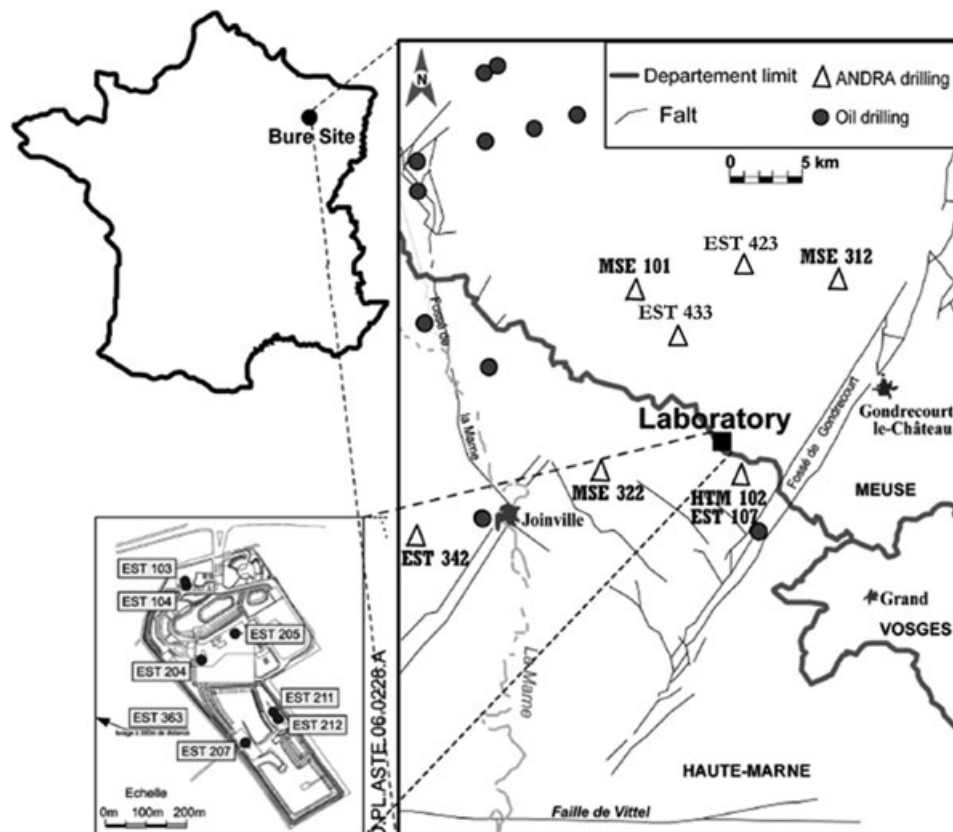


**Figure 1.** Location of the boreholes drilled by ANDRA where the core samples used in this study were extracted (modified from Trouiller 2006).

**Table 1.** Gravimetric water contents and porosities of the various Callovo–Oxfordian clay-rock units determined from the interpretation of borehole measurements (ANDRA 2008).

Unit	Gravimetric water content <sup>a</sup>		Porosity <sup>b</sup>	
	Mean (per cent)	Standard deviation	Mean (–)	Standard deviation
C2d	6.00	2.41	0.137	0.047
C2c	7.35	2.71	0.163	0.048
C2b2	8.04	1.03	0.178	0.019
C2b1	7.41	1.21	0.166	0.022
C2a	7.06	2.66	0.157	0.043
COx <sup>c</sup>	7.35	1.66	0.16	0.030

<sup>a</sup>Values obtained from a 150 °C reference (dry).

<sup>b</sup>Calculated from the gravimetric water content with  $\rho_w = 1000 \text{ kg m}^{-3}$  and  $\rho_g = 2690 \text{ kg m}^{-3}$ .

<sup>c</sup>Mean values of the Callovo–Oxfordian formation

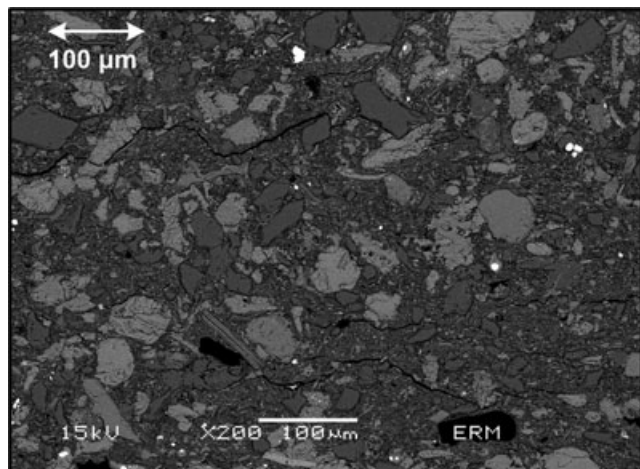


**Figure 2.** SEM (Scanning Electron Micrograph) picture of the Callovo–Oxfordian clay-rock (credit: J.C. Robinet, ERM). The picture shows grains of silica and carbonates (typical diameter comprised between 10 and 30  $\mu\text{m}$ ) and a clay matrix (in dark grey).

of the Callovo–Oxfordian formation corresponds to the C2a unit (<508 m). The mean gravimetric water contents and porosities of the different units are summarized in Table 1 (ANDRA 2005).

The Callovo–Oxfordian clay-rock can be conceptualized as a clay matrix with some imbedded grains of silica and carbonates (calcite and a minor fraction of dolomite). (Fig. 2). The clay matrix represents 20–50 per cent of the rock volume in the total formation (up to 45–50 per cent in the subunit C2b1). This clay fraction is mainly composed of illite and interstratified illite-smectite clays. There is also a small amount of kaolinite in the lower part of the formation. Smectite based clay-minerals form aggregates called tactoids. The size of the tactoid is typically 10  $\mu\text{m}$  (ANDRA 2005). The size of the silica and carbonate grains is usually larger than 4  $\mu\text{m}$  with a mean around 10–20  $\mu\text{m}$ . The volume of the silica and carbonate grains represent between 20 and 40 per cent of the rock assemblage. In addition, there are small amounts of potassic feldspar, plagioclase and pyrite. An extensive geochemical analysis of the Callovo–Oxfordian formation has been proposed recently by Gaucher *et al.* (2004).

### 3 THEORETICAL DEVELOPMENTS

#### 3.1 Theory

We consider a representative elementary volume of the Callovo–Oxfordian clay-rock of porosity  $\phi$ . The pore volume is

**Table 2.** Callovo–Oxfordian porewater composition.

THERMOAR model (Gaucher <i>et al.</i> 2006)		Simplified solute composition <sup>a</sup> (only charged species)	
Species	$C_i$ (mol L <sup>-1</sup> )	Species	$C_i$ (mol L <sup>-1</sup> )
Na	$32 \times 10^{-3}$	Na <sup>+</sup>	$31.5 \times 10^{-3}$
K	$7 \times 10^{-3}$	K <sup>+</sup>	$6.5 \times 10^{-3}$
Ca	$15 \times 10^{-3}$	Ca <sup>2+</sup>	$9.5 \times 10^{-3}$
Mg	$14 \times 10^{-3}$	Mg <sup>2+</sup>	$8.1 \times 10^{-3}$
Cl	$30 \times 10^{-3}$	Cl <sup>-</sup>	$30 \times 10^{-3}$
S(+6)	$34 \times 10^{-3}$	SO <sub>4</sub> <sup>2-</sup>	$21 \times 10^{-3}$
pH	7.3	–	–
pCO <sub>2</sub>	-2.51	HCO <sub>3</sub> <sup>-</sup>	$1.2 \times 10^{-3}$

<sup>a</sup>Obtained using PHREEQC2 (see Leroy *et al.* 2007). The software PHREEQC2 is described in Parkhurst & Appelo (1999).

filled by two continuous and immiscible fluid phases, a wetting fluid (subscript  $w$ ) and a non-wetting fluid. In our analysis, the wetting fluid is water and the non-wetting fluid is air. We denote  $s_w \in [0; 1]$  the saturation of the water phase. This saturation is related to the volumetric water content  $\theta$  by  $s_w = \theta/\phi$ . In soil science, many authors define also a gravimetric water content  $w$  defined as the ratio between the mass of the water phase  $m_w$  relative to the mass of the solid phase  $m_s$  of the core sample. Following Revil *et al.* (2007) and Revil & Jougnot (2008), we define a percolation threshold  $s_w^c$  for the water phase. Below this threshold, the water phase is not continuous at the scale of the representative elementary volume (see also Hunt & Ewing 2003 for the use of percolation theory in the context of this problem).

The minerals of the Callovo–Oxfordian clay-rock, especially the clay minerals, have negatively charged surface at the pH of the pore water (pH = 7.2, see Table 2; Leroy *et al.* 2007). To counterbalance this negative charge on the mineral surface, the pore water has an excess of cations (see Leroy *et al.* 2007 for a geochemical modelling of the pore water composition of the Callovo–Oxfordian clay-rock). These counterions are partitioned between the Stern layer, which is attached to the mineral surface, and the diffuse layer located inside the pore water phase (Fig. 3). In our modelling approach and in unsaturated condition, the Callovo–Oxfordian clay-rock is composed by three phases: (1) the solid phase, including the insulating minerals coated by the conductive Stern layer, (2) the water phase including the diffuse layer and locally some free electrolyte pockets in some macropores and (3) the non-wetting phase corresponding to air. Neglecting the surface charge of the air–water interface ( $S_{aw}$ ) (see Linde *et al.* 2007; Revil *et al.* 2007), the charge balance

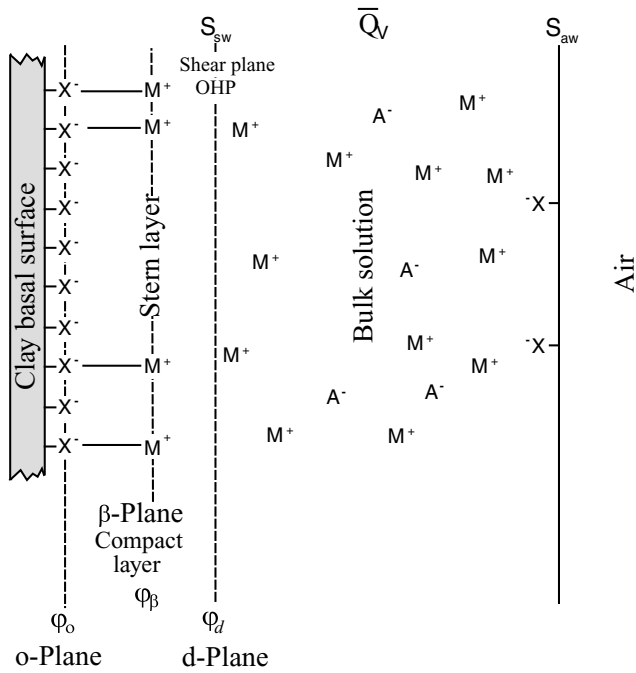


**Figure 3.** Sketch of the distribution of the ionic species in the pore space of a charged unsaturated porous medium. We note  $S_{sw}$  the shear plane between the mineral surface and the pore water and  $S_{wa}$  the interface between the air phase and the pore water (these two interfaces have complex shapes). The pore water is characterized by a volumetric charge density  $\bar{Q}_V$ .  $\varphi_0$ ,  $\varphi_\beta$  and  $\varphi_d$  are the electrical potentials of the surface of the mineral surface, the mid-plane of the  $\beta$ -Stern layer, and the shear plane, respectively. When the mean distance between the air/water interface and the mineral/water interface decreases, the ions of the pore water phase are confined in a smaller volume and therefore the conductivity of the pore water phase increases.

condition is

$$\frac{\bar{Q}_V}{s_w} + \frac{1}{V_w} S_{sw} Q_S = 0, \quad (1)$$

where  $Q_S$  is the total surface charge density (in  $\text{Cm}^{-2}$ ) at the solid-solution interface of area  $S_{sw}$  (including the true charge density on the mineral surface plus the surface charge density of the Stern layer),  $V_w$  (in  $\text{m}^3$ ) denotes the volume of the water phase and  $\bar{Q}_V/s_w$  represents the excess of charge per unit of volume of water in the unsaturated porous material ( $\bar{Q}_V$  is the volumetric charge density at saturation of the water phase). Considering a solution with  $Q$  ionic species  $i$ , the effective charge density of the pore water is written as

$$\frac{\bar{Q}_V}{s_w} = \sum_{i=1}^Q q_i \bar{C}_i, \quad (2)$$

where  $q_i$  is the charge ( $\pm z_i e$ , where  $z_i$  is the valency of the ion and  $e$  the charge of the electron, that is,  $\sim 1.6 \times 10^{-19}$  C) and  $\bar{C}_i$  the ionic concentration of the ion  $i$  in the medium bulk solution (in  $\text{m}^{-3}$ ). The bulk pore water solution of the clay matrix is mainly composed by the diffuse layer due to the small size of the pores (Leroy *et al.* 2007; Jougnot *et al.* 2009). We can use the Donnan approach to determine the ionic concentrations in the pore space of the clay matrix  $\bar{C}_i$  (Revil & Linde 2006; Leroy *et al.* 2007; Revil 2007). The ionic species that are present in the pore space of the clay-rock are assumed to be in local thermodynamic equilibrium with an infinite reservoir of the same  $Q$  ionic species at concentrations  $C_i$ .

Equilibrium implies (Revil & Linde 2006)

$$\bar{C}_i = C_i \exp\left(-\frac{q_i \varphi_m}{k_B T}\right), \quad (3)$$

where  $\varphi_m$  represents the mean electrical potential in the pore water phase (in V),  $k_B$  represents the Boltzmann constant ( $k_B = 1.3806 \times 10^{-23}$  JK $^{-1}$ ) and  $T$  is the absolute temperature (in K).

A very important parameter in the study of the electrical double layer is the partition coefficient  $f_Q$  (Leroy & Revil 2004; Leroy *et al.* 2007). This partition coefficient represents the fraction of the countercharge located in the Stern layer to compensate the true surface charge density of the mineral surface. We note  $\Gamma_{Xi}^0$  the surface site density of species  $i$  in the Stern layer and  $\Gamma_i^d$  the surface site density of species  $i$  in the diffuse layer (both in  $\text{m}^{-2}$ ). The partition coefficient  $f_Q$  is defined as (Leroy *et al.* 2007).

$$f_Q = \frac{\sum_{i=1}^Q z_i \Gamma_{Xi}^0}{\sum_{i=1}^Q z_i \Gamma_{Xi}^0 + \sum_{i=1}^Q z_i \Gamma_i^d}, \quad (4)$$

where  $z_i$  is the charge number of species  $i$ . For unsaturated conditions, the total charge density of counterions per unit of pore volume,  $Q_V$ , can be related to the excess of charge per unit of volume of solution in the medium,  $\bar{Q}_V/s_w$  and to the partition coefficient defined above by

$$\frac{\bar{Q}_V}{s_w} = (1 - f_Q) Q_V, \quad (5)$$

and  $Q_V$  can be related in turn to the cation exchange capacity (CEC, in C kg $^{-1}$ ) of the rock:

$$Q_V = \rho_s \left(\frac{1 - \phi}{\phi}\right) \text{CEC}, \quad (6)$$

where  $\rho_s$  is the bulk density of the solid phase of the material. The CEC characterizes the density of charge on the mineral surface because it can be measured directly using chemical titration methods. The electrical double layer theory developed by Leroy *et al.* (2007) includes a specific speciation model of the different crystalline planes of a mineral. This model can be used to infer the dependence of the partition coefficient  $f_Q$  with the ionic strength of the pore water,

$$I \equiv \frac{1}{2} \sum_{i=1}^Q z_i^2 \bar{C}_i. \quad (7)$$

Leroy & Revil (2009) proposed recently a model to study the spectral induced polarization of clay-rich porous materials saturated by water. This model is based on two different polarization mechanisms: (1) a polarization of the Stern layer associated with the discontinuity of the solid phase and (2) a Maxwell–Wagner polarization process. This model has been built for the case of a binary symmetric electrolyte (like NaCl or KCl). This is a major assumption of this study as discussed further below. Considering the composition of the pore water proposed by Gaucher *et al.* (2006) and Leroy *et al.* (2007) (see Table 2), we see that the sodium  $\text{Na}^+$  is the dominating counterion of the pore water. Therefore using a model with a single type of counterions is a reasonable assumption. However other counterions may be present and may play some role in widening the spectrum of the relaxation times. The sodium cation is located on the Outer Helmholtz Plane of the Stern layer, which is also called the d-plane (see Fig. 3), because sodium keeps its hydration shell on the mineral surface (Tournassat *et al.* 2009). Therefore it keeps some mobility along the mineral surface. If sodium would form an inner sphere complex with the mineral surface, it would have no tangential mobility along the mineral surface.

To extend the spectral induced polarization model developed by Leroy *et al.* (2007) to unsaturated conditions, and following Revil *et al.* (2007), we use the following change of variables to introduce the effect of the saturation of the water phase:  $1/F \rightarrow (s_w - s_w^c)^n / F$  and  $\bar{Q}_V \rightarrow \bar{Q}_V / s_w$  (see also Revil 1999), where  $F$  is the formation factor and  $n$  is the saturation exponent also called the second Archie's exponent (Archie 1942).

The polarization of the Stern layer is obtained by using the approach developed by Schwarz (1962). This approach is based on the assumption that there are no exchange of ions between the Stern and the diffuse layers. This assumption seems valid because the kinetics of ion sorption/desorption in the Stern layer is slow (typically several hours). We consider therefore that the movement of the ions in the Stern layer follows tangentially the pore water/mineral interface and that the characteristic length scale associated with this polarization mechanism is the size of the grains. In the model developed by Schwarz (1962), the relaxation time for the electromigration of an ion of species  $i$ ,  $\tau_i$  (in s), is therefore related to the particle radius  $a$  (in m) and to the diffusion coefficient of the ion  $i$  in the Stern layer  $D_S^i$  by,

$$\tau_i = \frac{a^2}{2D_S^i}. \quad (8)$$

This time constant corresponds to the relaxation time of the diffusion process of the counterions in the Stern layer with a characteristic distance  $a$ . In our model, the diffuse layer is homogenized with the pore water phase using the Donnan equilibrium approach (Revil & Linde 2006). We do not consider polarization for the diffuse layer because it forms a continuous phase through the porous material. In contrast, the Stern layer polarizes because it is discontinuous.

Because the clay fraction of the Callovo–Oxfordian clay-rock is mainly composed of illite and interstratified illite–smectite clays, we will consider only the response of illite and smectite to define the spectral induced polarization of the clay-rock. These minerals are coated by a Stern layer. We assume that all counterions are  $\text{Na}^+$ . If all grains had the same grain radius  $a_0$ , the Stern layer complex conductivity  $\bar{\sigma}_S$  could be computed by (Leroy & Revil 2009).

$$\bar{\sigma}_S(a_0, \omega) = \left( \frac{2\Sigma_S^\infty}{a_0} - \frac{2}{a_0} \frac{\Sigma_S^\infty}{(1 - i\omega\tau_{\text{Na}}^0)} \right), \quad (9)$$

with  $\omega$  the angular frequency (in  $\text{rad s}^{-1}$ ,  $\omega = 2\pi f$  is the frequency in Hertz),  $a_0$  is a grain size and  $\tau_{\text{Na}}^0$  is the associated relaxation time associated with the backdiffusion of the counterions in the Stern layer. At very low frequencies  $\omega \ll 1/\tau_{\text{Na}}^0$ , there is no contribution from the Stern layer to surface conductivity because of the diffusion of the counterions. At high frequencies, diffusion does not have the time to occur and therefore conductivity increases because of the contribution of the Stern layer conductivity. The parameter  $\Sigma_S^\infty$  corresponds therefore to the contribution of the Stern layer at high frequencies. This contribution is defined by (Leroy & Revil 2009).

$$\Sigma_S^\infty = e\beta_{\text{Na}}^S \Gamma_{\text{XNa}}^0, \quad (10)$$

(see also Revil *et al.* 1999; Revil & Leroy 2001) where  $e$  is the elementary charge,  $\beta_{\text{Na}}^S$  is the ionic mobility of the sodium in the Stern layer (in  $\text{m}^2 \text{s}^{-1} \text{V}^{-1}$ ). The mobility  $\beta_{\text{Na}}^S$  and the diffusion coefficient  $D_S^i$  are related to each other by the Nernst–Einstein relationship. The complex conductivity of the Stern layer  $\sigma_S^*$  (in  $\text{Sm}^{-1}$ ) is determined as (Leroy & Revil 2009).

$$\sigma_S^* = \bar{\sigma}_S + i\omega\varepsilon_s, \quad (11)$$

$$\varepsilon_s = 4.5\varepsilon_0, \quad (12)$$

where  $\varepsilon_s$  represents the dielectric permittivity of the clay minerals ( $\varepsilon_0 = 8.85 \times 10^{-12} \text{ Fm}^{-1}$ , the dielectric permittivity of vacuum). The effect of the grain size distribution is obtained by convoluting the response obtained for a single grain with the particle size distribution (PSD) (see Leroy & Revil 2009). The PSD is related to the distribution of the relaxation times through eq. (8).

The conductivity of the pore water needs to be computed accounting for the presence of  $Q$  ionic species and the effect of the diffuse layer. Generalizing the result obtained by Revil & Linde (2006) for the saturated case, the conductivity of the water phase (in  $\text{Sm}^{-1}$ ) in unsaturated condition is defined by,

$$\bar{\sigma}_f = \sum_{i=1}^Q q_i \beta_i \frac{\bar{C}_i}{s_w}, \quad (13)$$

where  $\beta_i$  is the ionic mobility of the species  $i$  in the solution (in  $\text{m}^2 \text{s}^{-1} \text{V}^{-1}$ ). We see therefore that the conductivity of the water phase depends strongly on the saturation of the water phase and increases with the saturation. A complex pore water conductivity  $\sigma_f^*$  can be defined as,

$$\sigma_f^* = \bar{\sigma}_f + i\omega\varepsilon_f, \quad (14)$$

with  $\varepsilon_f = 81\varepsilon_0$  the dielectric permittivity of water (at standard atmospheric pressure and at  $25^\circ\text{C}$ ).

We need now an expression for the conductivity of the representative elementary volume,  $\sigma^*$ , in unsaturated conditions. This is done by extending the result obtained by de Lima & Sharma (1992) and Revil *et al.* (2007) using the change of variable  $1/F \rightarrow (s_w - s_w^c)^n / F$  and  $\bar{Q}_V \rightarrow \bar{Q}_V / s_w$ . This yields,

$$\sigma^* = \frac{1}{F} [(s_w - s_w^c)^n \sigma_f^* + (F - 1) \sigma_S^*] \quad (15)$$

This model accounts for the Maxwell–Wagner polarization. This electrical conductivity model is part of the generalized framework proposed by Revil & Linde (2006) and Revil *et al.* (2007) to describe transport properties of saturated and unsaturated microporous media. This framework presents the important advantage to propose the determination of the macroscopic transport properties in a porous medium from a couple of intrinsic material properties that can be transposed from one macroscopic property to the other. From these fundamental properties, it becomes therefore possible to predict a wide variety of transport properties of the porous material (e.g. Jougnot *et al.* 2009 used the formation factor determined from electrical conductivity measurements to determine the diffusion coefficient of ionic tracers in core samples of the Callovo–Oxfordian clay-rock).

### 3.2 Sensitivity analysis

The previous model of induced polarization is based on seven independent parameters: (1) the formation factor,  $F$ , (2) the saturation index,  $n$ , (3) the percolation threshold,  $s_w^c$ , (4) the Donnan equilibrium potential,  $\varphi_m$ , (5) the surface site density of the counterions in the Stern layer,  $\Gamma_{\text{Na}}^0$  and (6) and (7) at least two parameters describing the grain size distribution (a mean and a standard deviation for a log normal probability distribution for instance).

The formation factor of the Callovo–Oxfordian clay-rock, in unit C2b1 and C2b2, is comprised between 15 and 140 (Jougnot *et al.* 2009). The saturation exponent  $n$  has been studied by Jougnot & Revil (2008) using a model for the thermal conductivity in unsaturated conditions that was applied to the Callovo–Oxfordian

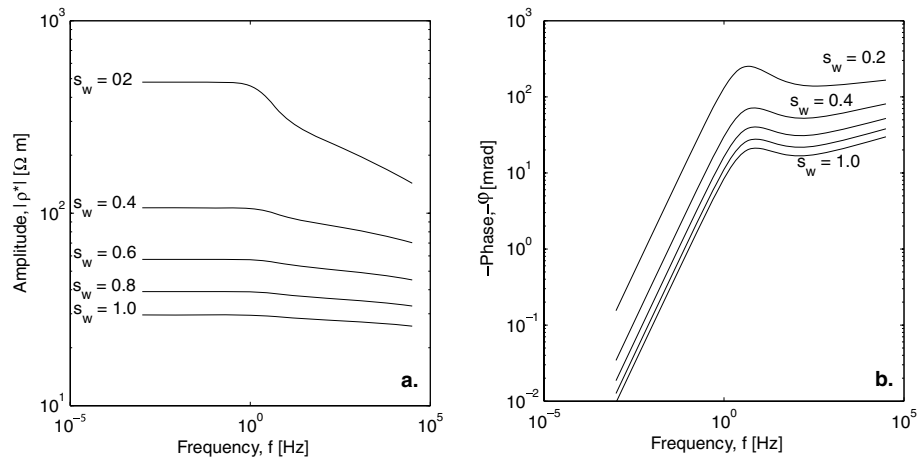


**Figure 4.** Sensitivity of the spectral induced polarization model with respect to the saturation of the water phase  $s_w$ . (a). Amplitude of the resistivity response versus frequency. (b). Phase versus frequency.

clay-rock. They obtained  $n = 2.0$ . No values exist for  $s_w^c$  for the Callovo–Oxfordian clay-rock. Revil & Jougnot (2008) previously considered  $s_w^c = 0.1$  as a reasonable value. We will see below that a correct estimate seems to be higher than this value. Considering the pore water composition determined by Gaucher *et al.* (2006) (the THERMOAR model reported in Table 2), the Donnan equilibrium potential,  $\varphi_m$ , is comprised between  $-54$  and  $-24$  mV (see Jougnot *et al.* 2009). From Leroy & Revil (2009), the surface site density,  $\Gamma_{Na}^0$ , is comprised between  $0.632 \text{ nm}^{-2}$  for pure smectite to  $1.12 \text{ nm}^{-2}$  for pure illite. The particle size distribution in consolidated clay-stones is difficult to determine experimentally because of the existence of the tactoids. As discussed above in Section 3.1, the distribution of the relaxation times,  $\tau$ , is related to the grain size distribution. We consider below a Cole–Cole distribution to characterize the distribution of the relaxation times (Cole & Cole 1941; Bötcher & Bordewijk 1978):

$$f(\tau) = \frac{1}{2\pi} \frac{\sin[\pi(c-1)]}{\cosh[c \ln(\tau/\tau_0)] - \cos[\pi(c-1)]}, \quad (16)$$

$$\int_0^\infty f(\tau) d\tau = 1, \quad (17)$$

where  $\tau_0$ , is the main relaxation time (in s) and  $c$  is the Cole–Cole exponent. This distribution is symmetric for  $\tau = \tau_0$ . Leroy & Revil (2009) obtained  $c = 0.76 \pm 0.05$  for the Mancos clay-rock and  $c \in [0.60; 0.84]$  for illites and smectites. This distribution is convoluted with the expression obtained for the Stern layer surface conductivity for a single grain, see eq. (9). In our model, the grain size distribution follows a Cole–Cole distribution and to this distribution is associated a distribution of relaxation time that follows also a Cole–Cole distribution. This is very different than taking an empirical Cole–Cole model to describe the modulus and the phase of the resistivity.

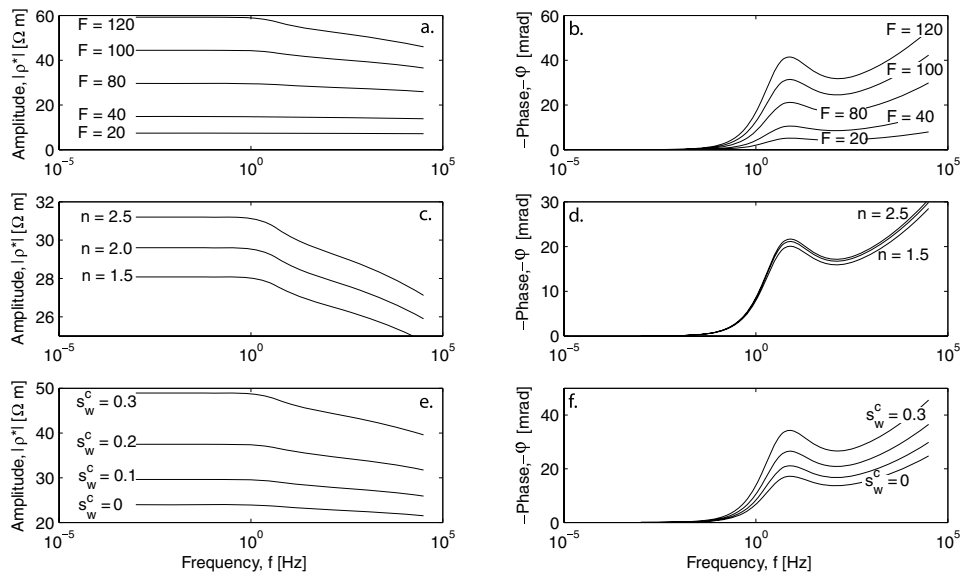
To perform a sensitivity analysis, the values of the seven key-parameters of our spectral induced polarization model can be chosen as follow:  $F = 80$ ,  $n = 2.0$ ,  $s_w^c = 0.10$ ,  $\varphi_m = -40$  mV,  $\Gamma_{Na}^0 = 1 \text{ nm}^{-2}$ ,  $c = 0.85$  (smectite-A in Leroy & Revil 2009) and  $\tau_0 = 3.80 \times 10^{-2}$  s (this corresponds to a grain diameter equal to  $10^{-5}$  m and an ionic mobility in the Stern layer of  $\beta_{Na}^S = 5.19 \times 10^{-8} \text{ m}^2 \text{ s}^{-1} \text{ V}^{-1}$ , according to eq. (8)). We present the spectral induced polarization data of our sensitivity test by showing the mod-

ulus of the complex resistivity  $|\rho^*|$  (the inverse of the complex conductivity in Ohm m) and the phase  $\varphi$  ( $\varphi = -\arctan[\text{Im}(\sigma^*)/\text{Re}(\sigma^*)]$ , in rad where  $\text{Im}(\sigma^*)$  represents the quadrature conductivity and  $\text{Re}(\sigma^*)$  represents the in phase conductivity). By convention, we will always plot  $(-\varphi)$  expressed in mrad.

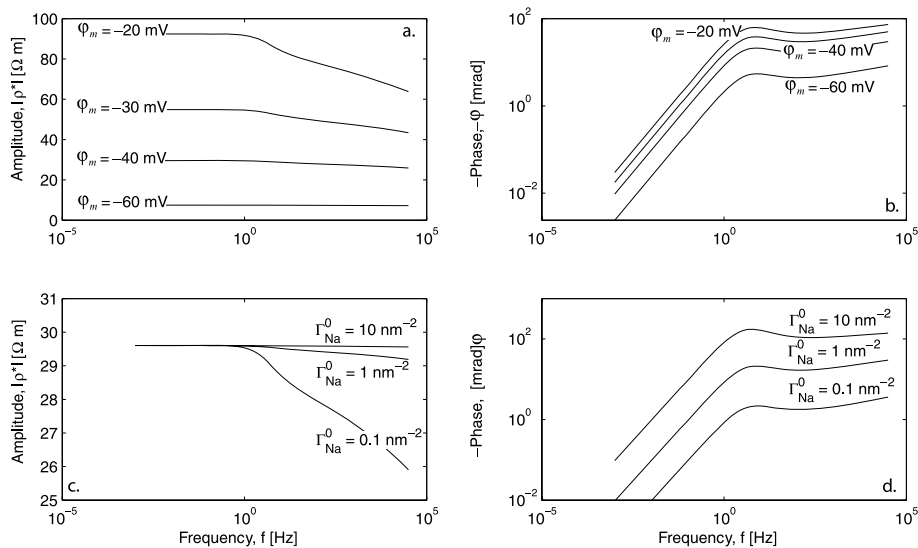
The first parameter we investigate is the saturation  $s_w$ . Fig. 4 shows the influence of the saturation with  $s_w \in \{0.2; 1\}$ . As expected, the amplitude of the complex resistivity increases with the desaturation of the porous material because of the insulating non-wetting phase (Fig. 4a). The phase also increases when the saturation decreases (Fig. 4b). This is because the presence of a non-wetting and insulating phase creates a new interface having an effect on the Maxwell–Wagner polarization. However, because the density of the counterions has also changed in the pore water, the presence of air has also an effect on the polarization of the Stern layer.

Fig. 5 shows the influence of  $F$ ,  $n$  and  $s_w^c$  upon the spectral induced polarization response of a clay-rock. All these parameters influence the response in the same way: when they increase, both the amplitude of the complex resistivity,  $|\rho^*|$  and the phase,  $-\varphi$ , increase (see Fig. 5). The sensitivity of our model to the two geochemical parameters ( $\varphi_m$  and  $\Gamma_{Na}^0$ ) is shown in Fig. 6. The Donnan equilibrium potential influences the signal in the same way as  $F$ ,  $n$  and  $s_w^c$ . The surface site density influences the model in a completely different way. When  $\Gamma_{Na}^0$  increases, the amplitude increases at high frequencies ( $>1$  Hz) but not at low frequency ( $<1$  Hz) where the phase decreases (Fig. 6). This implies that the effect of the surface site densities is different on the Maxwell–Wagner polarization, which dominates at high frequencies. This influence is made through the effect of surface conductivity, which changes the apparent conductivity of the grains. At low frequencies (below 10 Hz in the present case), the response is dominated by the polarization of the Stern layer.

We investigate now the influence of the distribution of the relaxation times by analysing the sensitivity of the model to the two parameters  $\tau_0$  and  $c$  (see Fig. 7). We note that the mean relaxation time and the Cole–Cole exponent influence the high frequency part of the amplitude ( $>10$  Hz) (Figs 7a and d).  $c$  also modifies the phase mainly at high frequency (Fig. 8b), while  $\tau_0$  completely shifts the peak of the phase. A lower value of  $\tau_0$  (smaller mean grain size or higher ionic mobility in the Stern Layer) corresponds to a shift of the critical frequency  $f_c$  to the high frequency [ $f_c = 1/(2\pi\tau_0)$ ]. A



**Figure 5.** Sensitivity analysis of the spectral induced polarization model with respect to the formation factor,  $F$ , the saturation index,  $n$  and the value of the critical water saturation,  $s_w^c$ . The frequency range investigated is comprised between 1 mHz and 10 kHz and the calculations are performed for a water-saturated material. (a, c, e) Amplitude of the resistivity versus frequency. (b, d, f) Phase versus frequency.



**Figure 6.** Influence of the two geochemical key parameters of the model (namely the Donnan equilibrium potential,  $\varphi_m$  (a and b), and the surface site density in the Stern layer,  $\Gamma_{Na}^0$ ) on the spectral induced polarization response for the frequency range 1 mHz–10 kHz at saturation. (a and c) Amplitude of the resistivity versus the frequency. (b and d) Phase versus the frequency.

lower value of  $c$  corresponds to a broader distribution of grain size. Consequently, this leads to a broader phase distribution, because the phase is strongly linked to the Stern layer polarization [the Stern layer contribution to the surface conductivity depends on the grain size, see eq. (9)].

## 4 EXPERIMENTAL MEASUREMENTS

### 4.1 Description of the rock samples

In the present contribution, we only study the spectral induced polarization response of Callovo–Oxfordian clay-rock sam-

ples. Due to the formation depth and the diagenetic phenomena, the Callovo–Oxfordian clay-stone is a very consolidated rock (ANDRA 2005) and samples do not fall apart after extraction. The samples used for the experiments have been extracted from the Callovo–Oxfordian layer at Bure (Meuse/Haute-Marne, France) by drilling with a NaCl saturated mud. The core samples have been extracted from the C2b1 and C2b2 units. The clay-rock has been sampled as a series of  $\sim 20$  cm long cylinders at different depths. The EST433 samples have been resampled to avoid the NaCl contamination and then became parallelepiped-like. All the samples have been conditioned in double hermetic aluminium bags and confined in polystyrene during the transport to avoid the perturbations. However a fraction of the samples have been broken during the

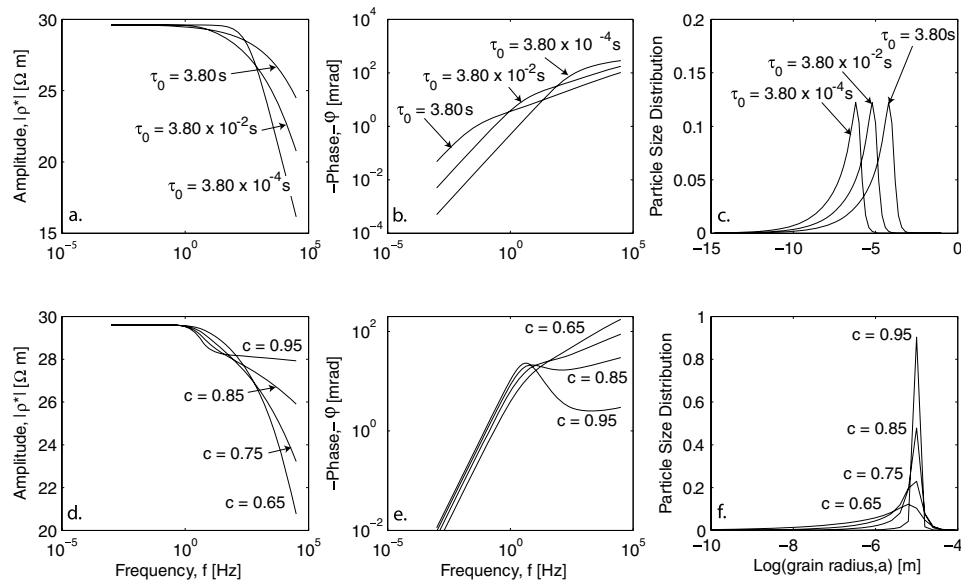


**Figure 7.** Influence of the two parameters controlling the particle size distribution (namely the mean relaxation time,  $\tau_0$  and the Cole–Cole exponent,  $c$ ) on the amplitude of the resistivity versus frequency and the phase versus frequency distributions. The sensitivity analysis is performed for the frequency range 1 mHz–10 kHz and for the saturated case ( $s_w = 1$ ). (a and d) Amplitude of the resistivity. (b and e) Phase. (c and f) Particle size distribution.

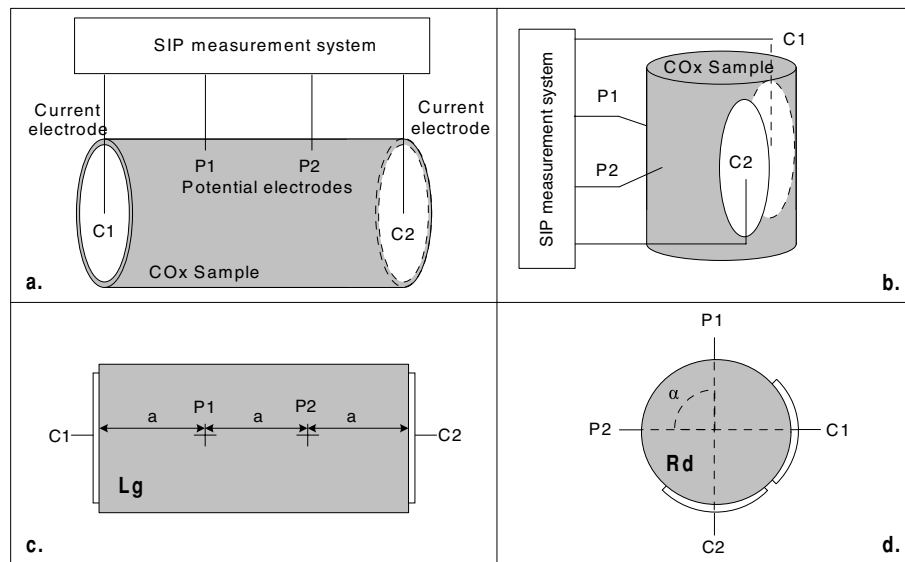


**Figure 8.** Experimental setups used for the spectral induced polarization measurements. (a, c) Sketch of the Lg-setup. Views from the side and the top, respectively. (b and d) Sketch of the Rg-setup. Views from the side and the top, respectively.

transportation. While opening, the samples were already partially unsaturated ( $s_w^i \in [0.75; 0.81]$ ). In order to limit the perturbation in the clay-stone pore space, we have decided not to resaturate the samples prior to our experiments. For the experiments, we used five samples from two boreholes at different depths (from units C2b1

and C2b2) and with different sizes (Table 3). We resampled some of the broken samples to make them usable for our experiments. Note that the resampling has been done with dry air to avoid sample pollution and/or osmotic perturbation (which could yield to the sample disintegration).

**Table 3.** Description of the core samples (the depth corresponds to the middle of the sample).

Sample	Borehole	Depth (m) <sup>a</sup>	Lithofacies	Length (m)	Diameter (m)
EST27906	EST423	518.16	C2b2	0.194	0.100
EST28144	EST423	582.16	C2b1	0.059	0.098
EST29296	EST433	617.52	C2b1	0.108	0.063
EST29300	EST433	624.38	C2b1	0.167	0.055
EST30749	EST433	608.07	C2b2	0.078	0.063

## 4.2 Experimental setup

The Spectral Induced Polarization method is based on the measurements of the complex resistivity  $\rho^*$  (in  $\Omega\text{m}$ ) over several decades of frequency (usually from 1 mHz to 10 kHz). The complex resistivity is the inverse of the complex conductivity:  $\rho^* = 1/\sigma^*$ . What is actually measured is the complex impedance  $Z^*$  (in  $\Omega$ ) between the end-faces of a cylindrical sample for instance (Pelton *et al.* 1983):

$$Z^*(\omega) = \frac{U}{I} = |Z^*(\omega)| e^{i\varphi(\omega)}, \quad (18)$$

where  $U$  is the voltage between the end-face boundaries of the sample,  $I$  the magnitude of the current which goes through the sample, and  $|Z^*(\omega)|$  and  $\varphi(\omega)$  are the amplitude and the phase of the complex impedance, respectively. The complex resistivity  $\rho^*$  is related to  $Z^*$  by a geometrical factor  $K$  (in m) by:  $\rho^*(\omega) = K Z^*(\omega)$ . This geometrical factor takes into account not only the position of the electrodes on the sample, but also the size and the shape of the samples. The complex resistivity  $\rho^*$  can be recasted into a modulus  $|\rho^*(\omega)|$  and a phase  $\varphi(\omega)$ . In the present contribution, amplitude will always stand for the resistivity amplitude. The phase is the same for the resistivity and the impedance.

Considering the geometry of samples #EST27906, #EST29296 and #EST29300, we choose the same electrode array than proposed by Cosenza *et al.* (2007). It is a Wenner- $\alpha$  type array (see Figs 8a and c for details). This setup is called the Lg-setup below. The lengths of samples #EST28144 and #EST30749 were too short to use the Lg-setup. Therefore, we tried a different approach by putting the electrodes on the side of the core samples (name the Rd-setup below). Instead of the length of the sample, we used a constant angle  $\alpha = 45^\circ$  between each electrode (see Figs 8b and d for details). Due to the orientation of the boreholes in the Callovo–Oxfordian formation, the Lg-setup corresponds to electrical measurements perpendicular to the stratification while the Rd-setup provides measurements parallel to the stratification.

Both setups are composed by two current electrodes (C1 and C2) and two potential electrodes (P1 and P2). All these electrodes were developed in the medical world. We found that they allow the best contact, and thus the lowest contact resistance, among various tested electrodes. The current (or source) electrodes are used to inject an alternative current at different frequencies. We choose the round 50 mm diameter electrodes to fit the different sample sizes. They have thin carbon films to improve the contact (Dura-Stick II). The potential electrodes are electrocardiogram (ECG) electrodes: their silver–silver chloride (Ag/AgCl) composition made them non-polarizable (3M Red Dot). Each of these electrodes correspond to a round 10 mm diameter metal disk, galvanized with silver and covered with a soft sponge imbibed of a AgCl gel. For the computation of the geometrical constant  $K$ , it is important to note that the current electrodes have a diameter of 50 mm while the potential electrodes are nearly punctual.

The non-polarizability of the potential electrodes has been validated using porous and electrically inert samples. For example, a clean (clay-free) limestone sample saturated with a saline NaCl brine ( $0.78 \text{ S m}^{-1}$  at  $25^\circ\text{C}$ ) was used to perform a test as prescribed by Vinegar & Waxman (1984). As predicted, we measured no significant polarization in this case (see Fig. 9).

Spectral induced polarization measurements were performed using the apparatus developed at the Central Laboratory for Electronics, ZEL, at the Forschungszentrum Jülich, in Germany (Zimmermann *et al.* 2008). It is based on a four-electrode system operating in the frequency range 1 mHz–45 kHz. To our knowledge,

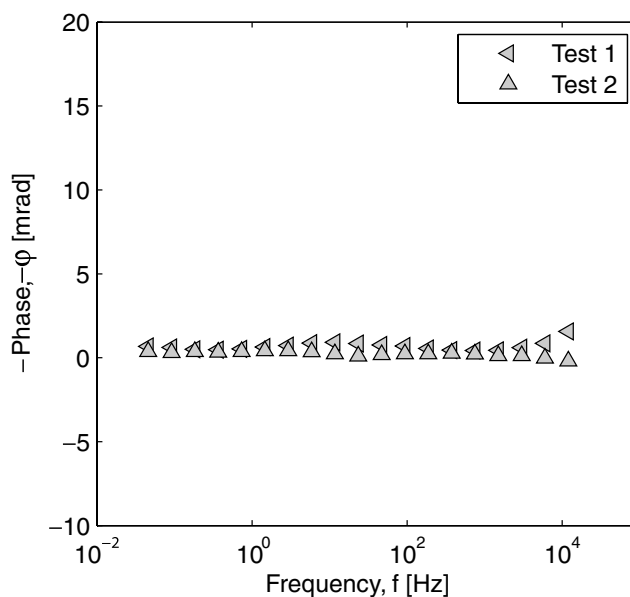


**Figure 9.** Test of the spectral induced polarization equipment and the electrodes (3M Red Dot) used to measure the potential response. This experiment is performed with a clean (clay-free) limestone sample saturated with a conductive brine (at  $0.78 \text{ S m}^{-1}$  at  $25^\circ\text{C}$ ). In this condition, we expect the phase to be close to zero in the investigated frequency range in agreement with the experimental data.

its accuracy is unmatched (0.1 mrad between 1 mHz and 1 kHz). We have tested the linearity of the system to check the influence of the input voltage on the measured currents (Fig. 10). This test shows that the spectral induced polarization mechanisms involved in these experiments are linear for applied voltage differences higher than 0.1 V. In all the experiment, we used  $U = 5 \text{ V}$  for the applied voltage.

For each electrode configuration set-up, we need to convert the measured resistance into a resistivity by using a geometrical coefficient, which depends on the position of the electrode, their extension, and the geometry of the sample. Considering the sample and the measurement setup (Lg or Rd) discussed above, we determined the values of  $K$  by solving the Laplace equation with source current terms using the finite element code COMSOL Multiphysics 3.4 accounting for the geometry of the core sample and the geometry of the electrodes discussed above. The values of these coefficients are reported in Table 4.

## 4.3 Drying procedure

We dried the core samples in two phases: (1) We call the first phase the desaturation phase while (2) the second phase is termed the heating phase (see Cosenza *et al.* 2007 and Ghorbani *et al.* 2009 for more details about this procedure). The studied samples were already partially unsaturated at the beginning of the experiments. We choose not to resaturate them to avoid possible perturbations like the swelling associated with changes in pore water composition. The saturations of the samples have been monitored through their weight with a precise balance ( $\pm 0.1 \text{ g}$ ). The sample water saturations have been calculated from:

$$s_w = \frac{w \rho_d}{\phi \rho_w}, \quad (19)$$

where  $w = (m_{\text{meas}} - m_d)/m_d$  is the gravimetric water content with  $m_{\text{meas}}$ , the measured mass, and  $m_d$ , the dry mass of the sample.  $\phi$

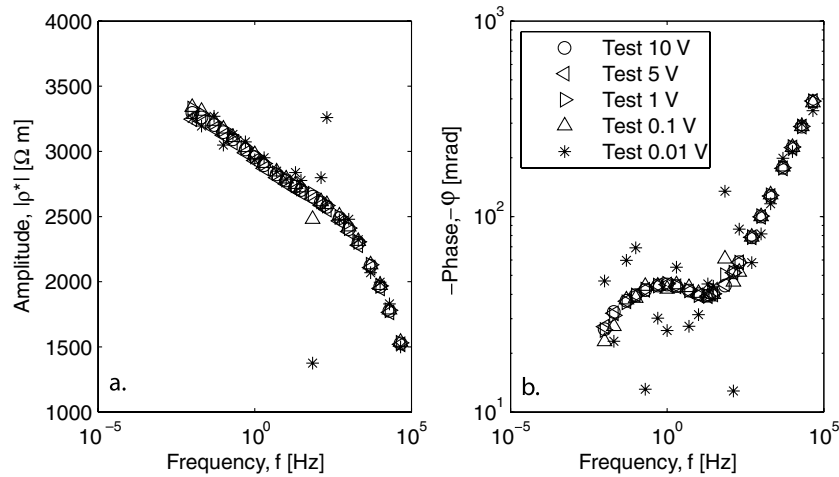


**Figure 10.** Linearity test of the equipment used to perform the spectral induced polarization measurements in the frequency range 10 mHz–45 kHz. We used a partially saturated Callovo–Oxfordian core sample EST29300. (a) Amplitude of the resistivity versus the frequency. (b) Phase versus the frequency. We used the following input voltages: 10, 5, 1, 0.1 and 0.01 V. Note that the response is independent on the applied voltage (at least for voltages higher than 1 V). The responses conform to the linear Ohm’s law.

**Table 4.** Properties of the samples and experimental setups.

Sample	Setup	Geometrical factor, $K$ (m)	Porosity, $\phi$ (-) <sup>a</sup>	Initial saturation, $s_w^i$ (-) <sup>b</sup>
EST27906	Lg	0.1219	0.157	0.805
EST28144	Rd	0.1756	0.176	0.797
EST29296	Lg	0.0913	0.163	0.770
EST29300	Lg	0.0703	0.146	0.748
EST30749	Rd	0.3835	0.181	0.808

<sup>a</sup>Values from TCMR measurement in the borehole at the sample depth (ANDRA).

<sup>b</sup>Values calculated from the weight measurements with the TCMR porosity.

is the ‘Total Combinable Magnetic Resonance’ (TCMR) porosity,  $\rho_w = 1000 \text{ kg m}^{-3}$ , and  $\rho_d = (1 - \phi)\rho_g$  are the water and the dry density, respectively (with  $\rho_g = 2690 \text{ kg m}^{-3}$  the grain density, see Gaucher *et al.* 2004 for details). We have decided to use the TCMR porosity (from borehole measurements) as a reliable estimate of the connected porosity because a study by ANDRA (2009) demonstrated that this was indeed the best estimate of the real porosity. The dry mass of the sample have been measured at the end of each experiment with the core samples being 24 hr at 105 °C in an oven. Table 4 presents the values of the porosity and the initial saturation,  $s_w^i$ , for each core sample.

We describe now quickly the desaturation phase. In this phase, the saturation decreases naturally by evaporation at  $T = 22 \pm 2$  °C and the relative humidity  $h_r = 22 \pm 4$  per cent. Spectral induced polarization measurements have been done at different times after we removed the protective bags of the core samples, thus at different levels of the water saturations. The second drying phase is called the ‘heating phase’ because the samples have been put into an oven for 24 hr at three different temperatures (70, 90 and 105 °C). The higher temperature allowed the measurement of the dry mass of the sample,  $m_d$ , for the saturation determination (see above). After each heating step, we have waited a couple of hours (typically 2–4 hr) before the spectral induced polarization measurements were performed. This is the time required for the sample to cool down at room temperature ( $T = 22 \pm 2$  °C). Fig. 11 shows the monitored saturation of the five samples during these two phases.

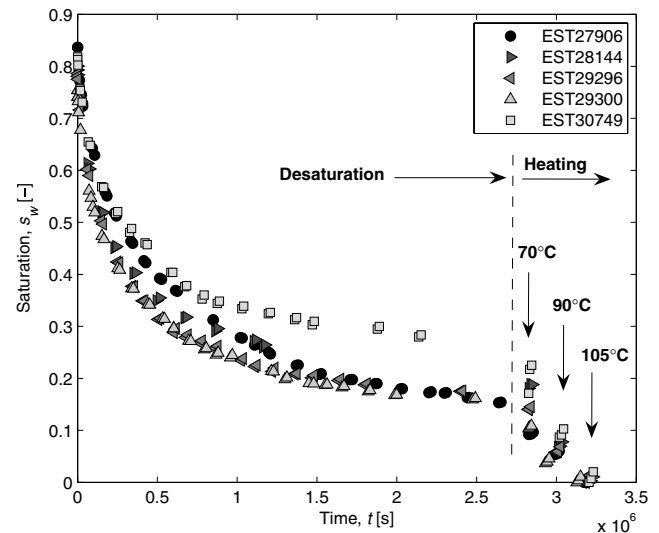


**Figure 11.** Complete desaturation curves for the five investigated samples as a function of the time and the three heating steps (70, 90 and 105 °C). Note the two phases for the desaturation: the desaturation phase and the heating phase.

## 5 INTERPRETATION

The spectral induced polarization signal can be decomposed into an amplitude  $|\rho^*|$  and a phase  $\phi$ . The behaviour of the amplitude can be compared to the DC resistivity except for the Stern contribution to surface conductivity (there is no contribution of the Stern layer at zero frequency according to the model described by Leroy *et al.* 2008 and Leroy & Revil 2009). We first analysed below the amplitudes (at a given low frequency) and then later the amplitude and the phase versus the frequency.

### 5.1 Interpretation of the amplitudes

We first focus on the amplitude of the complex resistivity at 10 Hz. We use the conductivity model developed by Revil *et al.* (2007) (eq. 15 above), which accounts for the saturation of the water phase. The conductivity of the pore water is calculated from the

THERMOAR geochemical model (see Table 2) and the Donnan equilibrium model discussed by Revil & Linde (2006). In this approach, the contribution of the diffuse layer is accounted for inside the conductivity of the pore water phase. Using a ‘non-DC’ input current, we have to consider the Stern contribution to the surface electrical conductivity  $\sigma_S$ . Therefore the conductivity model has five parameters:  $F$ ,  $n$ ,  $s_w^c$ ,  $\varphi_m$  and  $\sigma_S$ , which is itself determined from a grain size distribution. We determined the values of these five parameters for each core sample using the Simplex algorithm to solve a non-linear optimization procedure. This algorithm is able to optimize parameters value by minimizing a cost function  $G$  defined by the sum of the square residual between the  $N$  measured and calculated conductivities,  $\sigma_{\text{meas}}^k$  and  $\sigma_{\text{calc}}^k$ , respectively

$$\text{Min}G = \sum_{k=1}^N (\sigma_{\text{meas}}^k - \sigma_{\text{calc}}^k)^2. \quad (20)$$

This problem being well posed, we do not need any regularization term. Minimization is performed for both the real and the imaginary parts of the complex conductivity.

Fig. 12 shows that the Revil *et al.* (2007) model fit pretty well the experimental data with the optimized parameters given in Table 5. The optimized values of the different parameters agree with previous data obtained on core samples from the C2b1 and C2b2 units of the Callovo–Oxfordian formation. For example,  $F \in [38; 81]$  and

$\varphi_m \in [-49.5; -37.1]$  mV are consistent with the results obtained by Jougnot *et al.* (2009) and based on the diffusion of ionic tracers and *in situ* osmotic pressures in the Callovo–Oxfordian formation. The range of saturation exponents  $n \in [1.44; 2.04]$  is consistent with the values reported by Jougnot & Revil (2008) who developed a thermal conductivity model for unsaturated Callovo–Oxfordian clay-rocks. This model is an extension of the model developed by Revil (2000) to represent, in a unified framework, the electrical and thermal conductivities of granular media at saturation. The range of values of the saturation threshold  $s_w^c \in [0.10; 0.24]$  obtained from the conductivity measurements provide the first estimate of this parameter for the Callovo–Oxfordian clay-rock. The distribution of the surface conductivity associated with the Stern layer  $\sigma_S \in [0.96; 3.25] \times 10^{-5} \text{ S m}^{-1}$  is quite narrow. It is controlled by the density of counterions (sodium in the present case) in the Stern layer. As discussed further, this density is consistent with electrical triple layer calculations (see Leroy *et al.* 2007 and Leroy & Revil 2009).

The two experimental setups (Lg and Rd) have allowed measurements perpendicular and parallel to the bedding planes (Table 5). From these considerations, we see that anisotropy has an influence upon  $n$  and  $s_w^c$ . In fact, the value of  $n$  normal to the bedding is higher than the value of  $n$  parallel to the bedding plane. The opposite occurs for  $s_w^c$ . However these observations should be considered with caution. Indeed in the Rd-setup, the current electrodes are very close to each other. This geometry implies that the current lines are not

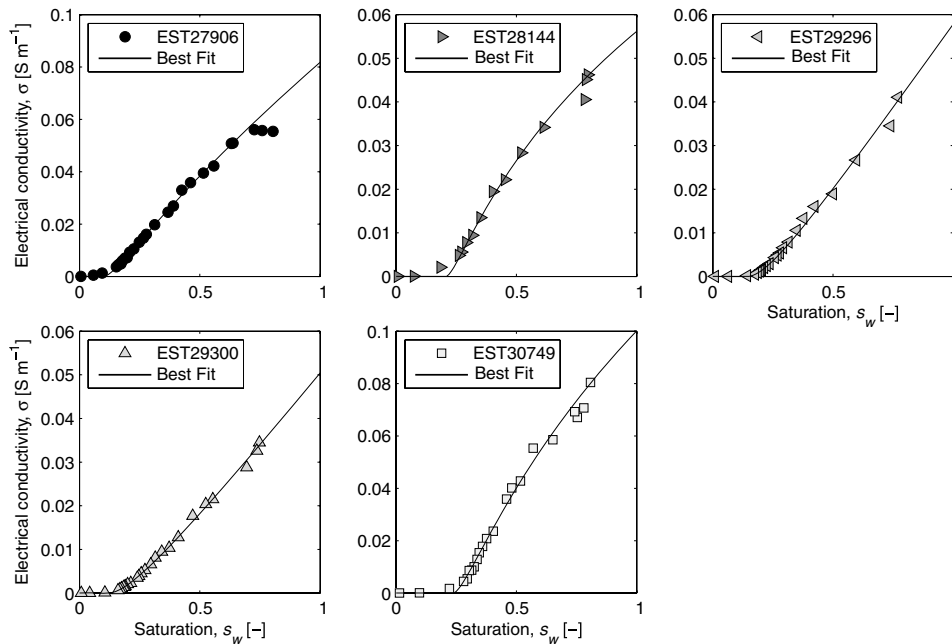


**Figure 12.** Comparison between the experimental data for the amplitude of the conductivity as a function of the saturation (measured at a frequency at 10 Hz). The plain line corresponds to the best fit obtained with the model proposed by Revil *et al.* (2007) (see main text). The uncertainties are smaller than the size of the symbols.

**Table 5.** Optimized values for the parameters entering the electrical conductivity model.

Sample	$F$ (-)	$n$ (-)	$s_w^c$ (-)	$\varphi_m$ (mV)	$\sigma_S$ ( $\text{S m}^{-1}$ )	Stratification
EST27906	44.6	1.79	0.10	-44.1	$1.01 \times 10^{-5}$	Normal
EST28144	80.7	1.44	0.21	-49.5	$1.33 \times 10^{-5}$	Parallel
EST29296	80.0	1.99	0.14	-49.4	$0.99 \times 10^{-5}$	Normal
EST29300	42.6	2.04	0.12	-37.1	$0.96 \times 10^{-5}$	Normal
EST30749	38.0	1.50	0.24	-48.0	$3.25 \times 10^{-5}$	Parallel

homogeneously distributed through each core sample and then the measurements may not be representative of the complete volume of the core samples. The only way to check these observations would be to make electrical measurements with the Lg-setup on core sampled parallel to the bedding planes. This has been done by Cosenza *et al.* (2007) using the Tournemire clay-rock but not in this work using the Callovo–Oxfordian clay-rock.

## 5.2 Amplitude and phase versus frequency

We consider now the whole set of complex resistivity data and compare it to our mechanistic model for unsaturated clay-rocks. Fig. 13 presents the measured data for the spectral induced polarization measurements on the sample #EST29300 at seven different saturations. We can note the similarity in this trend with our model prediction as shown in Fig. 4. Indeed, as expected, the amplitude and the phase increase when the saturation of the water phase decreases. We also observed that after the heating phases, the experimental data are noisy and characterized by high uncertainties (especially after the heating step at 105 °C), which makes them difficult to interpret (Fig. 13). This could be explained by the increase of the contact resistance between the electrodes and the surface of the core samples. In order to avoid misinterpretation of our results, we focus below only with the experiments performed with the Lg-setup excluding the data obtained in the heating phase (samples #EST27906, #EST29296 and #EST29300). In addition, in the heating phase, the formation of microcracks was observed and this creates a strong response upon the spectral induced polarization data (Cosenza *et al.* 2007; Ghorbani *et al.* 2009) and the presence of these microcracks has not yet been accounted for in our model.

In order to compare the experimental data and the proposed model for spectral induced polarization in unsaturated clay-rocks, we need to determine the unknown parameters of the model. In the previous section, we have determined four of the seven key parameters for the

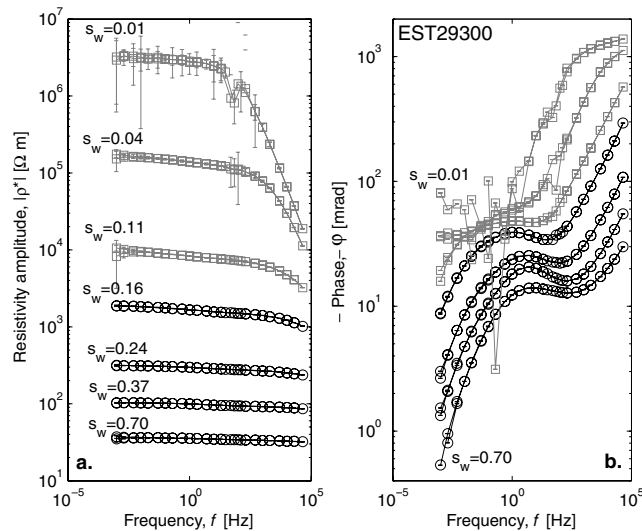


**Figure 13.** Experimental spectral induced polarization data (sample EST29300) at seven different saturations of the water phase and for the frequency range 1 mHz–45 kHz. (a) Amplitude of the resistivity versus the frequency. (b) Phase versus frequency. The black lines and open circles represent the data obtained during the desaturation phase (values of the water saturations:  $s_w = 0.70, 0.37, 0.24$  and  $0.16$ ). The grey lines and the grey open squares correspond to the heating phase ( $s_w = 0.11, 0.04$  and  $0.01$ ).

five core samples:  $F, n, s_w^c$  and  $\varphi_m$  (the values of these parameters are reported in Table 5). We used Leroy & Revil (2009) measurements in saturated clay-rich porous media for the three other parameters ( $\Gamma_{Na}^0, \tau_0$  and  $c$ ). These sets of values are considered to be prior values in the following. In order to find the best fit for each measurement, thus for the different saturations, we used a simple trial and error method from the prior parameters. Note that we optimize the whole complex signal: amplitude and phase at the same time.

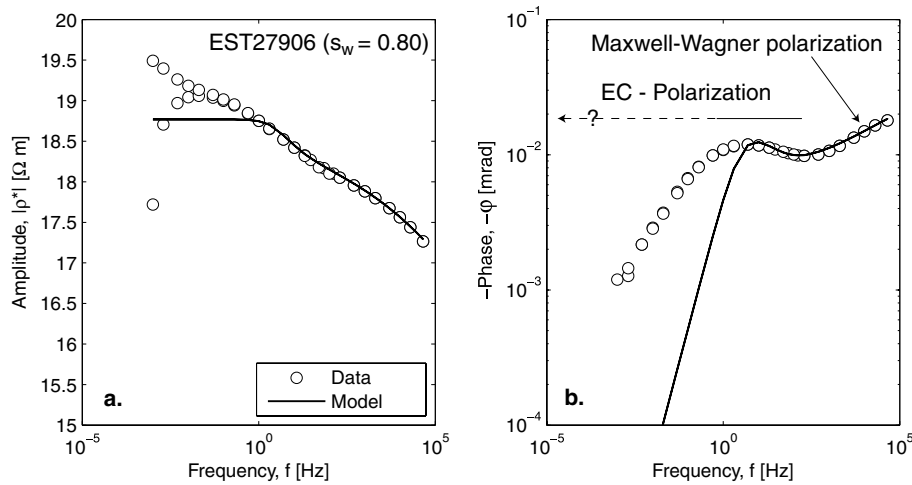
The measurements on the sample #EST27906 (at  $s_w = 0.82$ ) have been fitted by the proposed model with the following parameters:  $F = 54.5, n = 1.79, s_w^c = 0.10, \varphi_m = -44.1$  mV,  $\Gamma_{Na}^0 = 0.891$  nm<sup>-2</sup>,  $\tau_0 = 3.46 \times 10^{-2}$  s and  $c = 0.855$ . Fig. 14 shows that our model is able to fit pretty well the measured complex resistivities (total rms = 4.18 per cent with equal weight given to the in phase and quadrature conductivities). Dividing the frequency range in two parts, we see that the model perfectly fits the amplitude and the phase for frequencies higher than 1 Hz (Leroy *et al.* 2008; Leroy & Revil 2009). At lower frequencies, the predicted amplitudes are still pretty close to the experimental data, but the modelled phase underpredicts the data.

Fig. 15 shows the comparison between the measurements, during the desaturation procedure, and the prediction of the model. At low saturations, the measured Maxwell–Wagner polarization is higher than predicted by the model (from 1 to 15 kHz). The measured polarization is very well fitted between 1 Hz and 1 kHz.

Three explanations could explain the observed mismatch at low frequencies. (1) Another mechanism (like membrane polarization, see discussion in Leroy & Revil 2009) may occur at low frequencies and has not been accounted for in our model. (2) A second possibility is that we have only considered sodium as the only counterion responsible for the polarization of the Stern layer. Maybe this assumption is too restrictive. Other cations are sorbed and may participate to the polarization of the Stern layer broadening the distribution of the relaxation times of the polarization of this layer in the frequency domain. (3) We have considered an unimodal distribution of the relaxation time distribution. However, the distribution of the relaxation times may be multimodal (e.g. Ghorbani *et al.* 2009 used a double Cole–Cole model to fit their data). The mean relaxation time,  $\tau_0$ , corresponds to a grain radius of 9.5  $\mu$ m consistent both with the size of the tactoids and the size of the silica and carbonates grains.

The estimates of the model parameters determined by the best fits between the model and the data for core samples #EST27906, #EST29296 and #EST29300, are displayed in Fig. 16 as a function of the saturation. Note that the values of  $n, s_w^c$  and  $\varphi_m$  optimized using the amplitude data at 10 Hz gave the best fit (Table 5). The optimized values of  $F$  and  $c$  are independent on the saturation (see Figs 16a and b, respectively). This is consistent with the fact that the formation factor characterizes the topology of the pore space (Revil & Cathles 1999) and the exponent  $c$  characterizes the broadness of the grain size distribution (Leroy *et al.* 2008). The mean values of the formation factor are  $\bar{F} = 46.1 \pm 1.8, 85.5 \pm 5.1$  and  $44.1 \pm 2.2$  for the core samples #EST27906, #EST29296 and #EST29300, respectively. These values are consistent with those reported in Table 5. The mean values of the Cole–Cole exponents are  $\bar{c} = 0.852 \pm 0.005, 0.854 \pm 0.009$  and  $0.827 \pm 0.006$ , for the core samples #EST27906, #EST29296 and #EST29300, respectively.

We found that  $\tau_0$  and  $\Gamma_{Na}^0$  vary slightly with the saturation. Fig. 16(c) shows that  $\tau_0$  increases when the saturation decreases. This observation is consistent with one the two  $\tau$  of the fit by a double Cole–Cole model in the work of Ghorbani *et al.* (2009).



**Figure 14.** Comparison between the EST27906 measurement and the proposed model (for  $s_w = 0.80$ ): (a) Amplitude versus frequency. (b) Phase versus frequency (from 1 mHz to 45 kHz) (rms = 4.18 per cent). The Maxwell–Wagner polarization dominates at frequencies higher than 1 kHz. Below 1 kHz, the induced polarization response of the core sample is dominated by the polarization of the Stern layer. EC stands for the electrochemical polarization of the Stern layer.

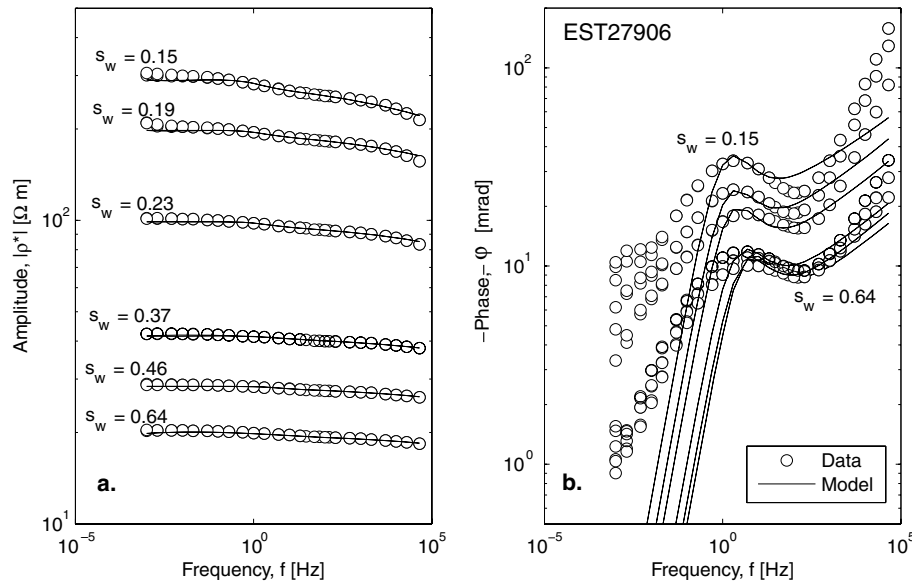


**Figure 15.** Comparison between the spectral induced polarization measurements from 1 mHz to 45 kHz (sample EST27906) and the proposed model (at six different saturations of the water phase). (a) Amplitude of the complex resistivity versus frequency. (b) Phase versus frequency. The plain lines correspond to the model predictions.

Ghorbani *et al.* (2009) explain this variation by textural changes. In fact, the clay mineral deformation (shrinkage) might break Stern layer connection inside the tactoids, and then increase the Stern layer diffusion path, thus the relaxation time. These results could confirm that the polarization of the Stern layer occurs in the tactoids and not around the coarse grains. This implies that the relaxation time distribution in such complex medium does not correspond directly to the particle size distribution, but more to a Stern diffusion path distribution inside the clay aggregates. In that case,  $\tau$  would not be related to the grain radii but to the characteristic length of the tactoids. This explanation seems to be more realistic considering the complex geometry of clay assembly in consolidated clay-rocks (see Montes *et al.* 2004 for Scanning Electron Microscope pictures of the Callovo–Oxfordian at 10 and 50  $\mu$ m scale). We observe also that the surface site density of sodium counterions in the Stern layer diminishes when the water saturation decreases.

This could be due to the disconnection of the Stern layers inside the tactoid.

## 6 CONCLUSIONS

We proposed a mechanistic model of spectral induced polarization to unsaturated clay-rocks. Sensitivity tests were conducted to determine the influence of saturation and seven key parameters on the modulus and phase of the complex resistivity. The model was successfully tested against experimental data on partially saturated core samples from the Callovo–Oxfordian formation. The model agreed with the amplitude of the conductivity (at 10 Hz) as a function of saturation. Then, we showed that the model was able to reproduce the complex conductivity behaviour of the medium at high frequencies ( $> 1$  Hz) for water saturations comprised between 0.2 and 0.8. The polarization of the Stern layer that seems to take

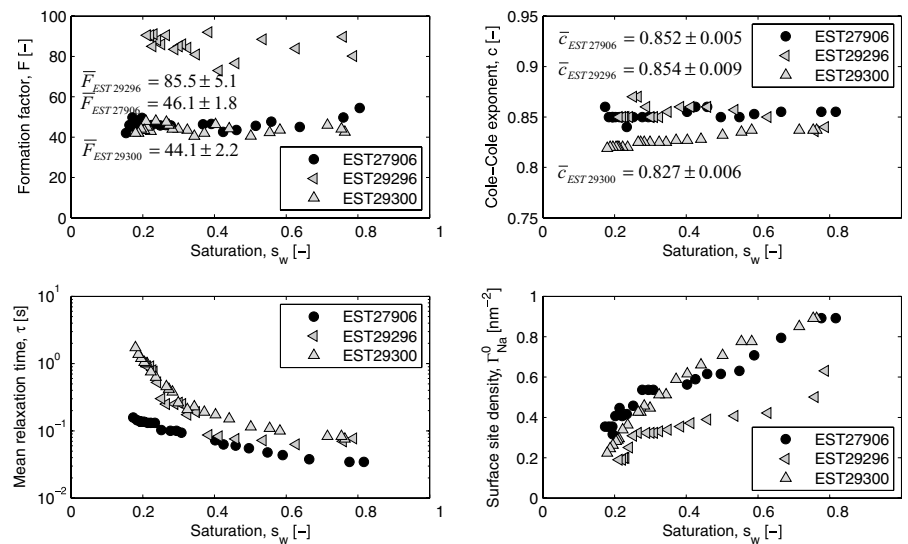


**Figure 16.** Evolution of the optimized model parameters as a function of the saturation: (a) the formation factor,  $F$ , (b) the Cole–Cole exponent,  $c$ , (c) the mean relaxation time,  $\tau$  and (d) the surface site density,  $\Gamma_{Na}^0$ . Note that the optimized values of  $n$ ,  $s_w^c$  and  $\varphi_m$  are constant for all the saturations. The dependence of the relaxation time with the saturation is opposite to that observed by Binley *et al.* (2005).

place at the scale of clay aggregates (tactoids) is related to a characteristic length that depends on the saturation of the water phase. In a future work, we will take into consideration the polarization of the Stern by several counterions with different valences and mobilities. In our opinion that would allow us to improve the fit at low frequencies ( $< 1$  Hz). We will also take into account the membrane polarization mechanism to produce a more complete theory.

## ACKNOWLEDGMENTS

We thank the French National Agency for Radioactive Waste Management (ANDRA) for its support. The Ph.D. thesis of Damien Jougnot is supported by ANDRA. D. Jougnot strongly thanks S. Altmann, D. Coelho and J.C. Robinet for fruitful discussions. A. Revil and D. Jougnot thank T. Young for his support at CSM and M. Batzle for his advices, and G. Okay for her help. We thank Andreas Weller, an anonymous referee and the Associate Editor Jörg Renner for the quality of the constructive comments and the speed of the review process.

## REFERENCES

- ANDRA, 2005. Dossier 2005 argile–Référentiel du site de Meuse/Haute Marne, Internal Report ANDRA n°C.RP.ADS.04.0022.
- ANDRA, 2008. Porosité totale des argilites du Callovo-Oxfordien, Internal Report ANDRA n°KMFIAEAP080032.
- ANDRA, 2009. Dossier 2009 Argile, Référentiel du site de Meuse Haute-Marne, Internal report ANDRA.
- Archie, G.E., 1942. The electrical resistivity log as an aid in determining some reservoir characteristics, *Trans. AIME*, **146**, 54–62.
- Binley, A., Slater, L.D., Fukes, M. & Cassiani, G., 2005. Relationship between spectral induced polarization and hydraulic properties of saturated and unsaturated sandstones, *Water Resour. Res.*, **41**, W12417, doi:10.1029/2005WR004202.
- Blaschek, R., Hördt, A. & Kemna, A., 2008. A new sensitivity-controlled focusing regularization scheme for the inversion of induced polarization data based on the minimum gradient support, *Geophysics*, **73**, F45–54.
- Börner, F.D., Schopper, J.R. & Weller, A., 1996. Evaluation of transport and storage properties in the soils and groundwater zone from

- induced polarization measurements, *Geophys. Prospect.*, **44**, 583–601, doi:10.1111/j.1365-2478.1996.tb00167.x.
- Böttcher, C.J.F. & Bordewijk, P., 1978. *Theory of Electric Polarization*, Vol. II, Dielectrics in Time-Dependent Fields, Elsevier Science, Amsterdam.
- Chen, J., Kemna, A. & Hubbard, S.S., 2008. A comparison between Gauss-Newton and Markov-chain Monte Carlo-based methods for inverting spectral induced-polarization data for Cole-Cole parameters, *Geophysics*, **73**, 247–258.
- Cole, K.S. & Cole, R.H., 1941. Dispersion and adsorption in dielectrics (I), *J. Chem. Phys.*, **9**, 341–351.
- Cosenza, P., Ghorbani, A., Florsch, N. & Revil, A., 2007. Effects of drying on the low-frequency electrical properties of Tournemire argillites, *Pure appl. Geophys.*, **164**, 2043–2066, doi:10.1007/s00024-007-0253-0.
- Cosenza, P., Ghorbani, A., Revil, A., Zamora, M., Schmutz, M., Jougnot, D. & Florsch, N., 2008. A physical model of the low-frequency electrical polarization of clay-rocks, *J. geophys. Res.*, **113**, B08204, doi:10.1029/2007JB005539.
- Davidson, D.W. & Cole, R.H., 1950. Dielectric relaxation in glycerine, *J. Chem. Phys.*, **18**, 1417.
- de Lima, O.A.L. & Niwas, S., 2000. Estimation of hydraulic parameters of shaly sandstone aquifers from geoelectrical measurements, *J. Hydrol.*, **235**, 12–26, doi:10.1016/S0022-1694(00)00256-0.
- de Lima, O.A.L. & Sharma, M.M., 1990. A grain conductivity approach to shaly sandstones, *Geophysics*, **55**, 1347–1356.
- de Lima, O.A.L. & Sharma, M.M., 1992. A generalized Maxwell-Wagner theory for membrane polarization in shaly sands, *Geophysics*, **57**(3), 431–440, doi:10.1190/1.1443257.
- Gaucher, E. *et al.*, 2004. ANDRA underground research laboratory: interpretation of the mineralogical and geochemical data acquired in the Callovo-Oxfordian Formation by investigative drilling, *Phys. Chem. Earth*, **29**, 55–77, doi:10.1016/j.pce.2003.11.006.
- Gaucher, E. *et al.*, 2006. Modeling the porewater chemistry of the Callovo-Oxfordian formation at a regional scale, *C. R. Geosci.*, **338**(12–13), 917–930.
- Ghorbani, A., Camerlynck, C., Florsch, N., Cosenza, P.H., Tabbagh, A. & Revil, A., 2007. Bayesian inference of the Cole-Cole parameters from time and frequency-domain induced polarization, *Geophys. Prospect.*, **55**(4), 589–605, doi:10.1111/j.1365-2478.2007.00627.x.
- Ghorbani, A., Cosenza, P.H., Revil, A., Zamora, M., Schmutz, M., Florsch, N. & Jougnot, D., 2009. Non-invasive monitoring of water content and textural changes in clay-rocks using spectral induced

- polarization: a laboratory investigation, *Appl. Clay Sci.*, **43**, 493–502, doi:10.1016/j.clay.2008.12.007.
- Homand, F., Giraud, A., Escoffier, S., Koriche, A. & Hoxha, D., 2004. Permeability determination of a deep argillite in saturated and partially saturated conditions, *Int. J. Heat Mass Transfer*, **48**, 3517–3531.
- Hördt, A., Blaschek, R., Kemna, A. & Zisser, N., 2007. Hydraulic conductivity estimation from induced polarisation data at the field scale—the Krauthausen case history, *J. appl. Geophys.*, **62**, 33–46.
- Hunt, A.G. & Ewing, R.P., 2003. On the vanishing of solute diffusion in porous media at a threshold moisture content, *Soil Sci. Soc. Am. J.*, **67**, 1701–1702.
- Jougnot, D. & Revil, A., 2008. Thermal conductivity of unsaturated clay-rocks, *Hydrol. Earth Syst. Sci. Discuss.*, **5**, 2409–2423.
- Jougnot, D., Revil, A. & Leroy, P., 2009. Diffusion of ionic tracers in the Callovo-Oxfordian clay-rock using the Donnan equilibrium model and the formation factor, *Geochim. Cosmochim. Acta*, **73**, 2712–2726, doi:10.1016/j.gca.2009.01.035.
- Kemna, A., Binley, A., Ramirez, A. & Daily, W., 2000. Complex resistivity tomography for environmental applications, *Chem. Eng. J.*, **77**, 11–18.
- Kemna, A., Binley, A. & Slater, L., 2004. Crosshole IP imaging for engineering and environmental applications, *Geophysics*, **69**, 97–107.
- Kruschwitz, S. & Yaramanci, U., 2004. Detection and characterization of the disturbed rock zone in claystone with complex resistivity method, *J. appl. Geophys.*, **57**, 63–79, doi:10.1016/j.jappgeo.2004.09.003.
- Leroy, P. & Revil, A., 2004. A triple layer model of the surface electrochemical properties of clay minerals, *J. Colloid Interface Sci.*, **270**(2), 371–380.
- Leroy, P. & Revil, A., 2009. A mechanistic model for the spectral induced polarization of clay material, *J. geophys. Res.*, **114**, B10202, doi:10.1029/2008JB006114.
- Leroy, P., Revil, A., Altmann, S. & Tournassat, C., 2007. Modeling the composition of the pore water in a clay-rock geological formation (Callovo-Oxfordian, France), *Geochim. Cosmochim. Acta*, **71**(5), 1087–1097, doi:10.1016/j.gca.2006.11.009.
- Leroy, P., Revil, A., Kemna, A., Cosenza, P. & Ghorbani, A., 2008. Spectral induced polarization of water-saturated packs of glass beads, *J. Colloid Interface Sci.*, **321**, 103–117, doi:10.1016/j.jcis.2007.12.031.
- Lesmes, D.P. & Morgan, F.D., 2001. Dielectric spectroscopy of sedimentary rocks, *J. geophys. Res.*, **106**, 13 329–13 346, doi:10.1029/2000JB900402.
- Linde, N., Jougnot, D., Revil, A., Matthäi, S., Arora, T., Renard, D. & Doussan, C., 2007. Streaming current generation in two phase flow conditions, *Geophys. Res. Lett.*, **34**, L03306, doi:10.1029/2006GL028878.
- Marshall, D.J. & Madden, T.R., 1959. Induced polarization: a study of its causes, *Geophysics*, **24**(4), 790–816, doi:10.1190/1.1438659.
- Montes, H.G., Duplay, J., Martinez, L., Escoffier, S. & Rousset, D., 2004. Structural modifications of Callovo-Oxfordian argillite under hydration/dehydration conditions, *Appl. Clay Sci.*, **25**, 187–194.
- Parkhurst, D.L. & Appelo, C.A.J., 1999. User's guide to PHREEQC (Version 2)—a computer program for speciation, batch-reaction, one-dimensional transport, and inverse geochemical calculations: U.S. Geological Survey Water-Resources Investigations Report 99–4259, 312 p.
- Pelton, W.H., Sill, W.R. & Smith, B.D., 1983. Interpretation of complex resistivity and dielectric data, Part I, *Geophys. Trans.*, **29**(4), 297–330.
- Pusch, R., 2006. Clays and nuclear waste management, in *Handbook of Clay Science*, pp. 703–716, eds Bergaya, F., Theng, B.K.G. & Lagaly, G., Elsevier, Amsterdam.
- Revil, A., 1999. Ionic diffusivity, electrical conductivity, membrane and thermoelectric potentials in colloids and granular porous media: a unified model, *J. Colloid Interface Sci.*, **212**, 503–522.
- Revil, A., 2000. Thermal conductivity of unconsolidated sediments with geophysical applications, *J. geophys. Res.*, **105**, 16,749–16,768.
- Revil, A., 2007. Thermodynamics of transport of ions and water in charged and deformable porous media, *J. Colloid Interface Sci.*, **307**(1), 254–264.
- Revil, A. & Cathles, L.M., 1999. Permeability of shaly sands, *Water Resour. Res.*, **35**(3), 651–662.
- Revil, A. & Jougnot, D., 2008. Diffusion of ions in unsaturated porous materials, *J. Colloid Interface Sci.*, **319**, 226–235, doi:10.1016/j.jcis.2007.10.041.
- Revil, A. & Leroy, P., 2001. Hydroelectric coupling in a clayey material, *Geophys. Res. Lett.*, **28**(8), 1643–1646.
- Revil, A. & Leroy, P., 2004. Governing equations for ionic transport in porous shales, *J. geophys. Res.*, **109**, B03208, doi:10.1029/2003JB002755.
- Revil, A. & Linde, N., 2006. Chemico-electromechanical coupling in microporous media, *J. Colloid Interface Sci.*, **302**, 682–694, doi:10.1016/j.jcis.2006.06.051.
- Revil, A., Pezard, P.A. & Glover, P.W.J., 1999. Streaming potential in porous media. 1. Theory of the zeta-potential, *J. geophys. Res.*, **104**(B9), 20,021–20,031.
- Revil, A., Linde, N., Cerepi, A., Jougnot, D., Matthäi, S. & Finsterle, S., 2007. Electrokinetic coupling in unsaturated porous media, *J. Colloid Interface Sci.*, **313**, 315–327, doi:10.1016/j.jcis.2007.03.037.
- Schwarz, G., 1962. A theory of the low-frequency dielectric dispersion of colloidal particles in electrolyte solution, *J. Phys. Chem.*, **66**, 2636–2642.
- Slater, L. & Binley, A., 2006. Synthetic and field-based electrical imaging of a zero valent iron barrier: implications for monitoring long-term barrier performance, *Geophysics*, **71**, B129–137.
- Tabbagh, A., Cosenza, P.H., Guérin, R., Ghorbani, A. & Florsch, N., 2009. Modelling of Maxwell-Wagner induced polarisation amplitude, *J. appl. Geophys.*, **67**(2), 109–113.
- Tournassat, C., Chapron, Y., Leroy, P., Bizi, M. & Boulahya, F., 2009. Comparison of molecular dynamics simulations with Triple Layer and modified Gouy-Chapman models in a 0.1 M NaCl – montmorillonite system, *J. Colloid Interface Sci.*, **339**, 533–541, doi:10.1016/j.jcis.2009.06.051.
- Trouiller, A., 2006. The Callovo-Oxfordian of the Paris Basin: from its geological context to the modelling of its properties, *C. R. Geosci.*, **338**, 815–823.
- Tsang, C.-F., Bernier, F. & Davies, C., 2005. Geohydronechanical processes in the Excavation Damaged Zone in crystalline rock, rock salt, and indurated and plastic clays in the context of radioactive waste disposal, *Int. J. Rock Mech. Min. Sci.*, **42**, 109–125, doi:10.1016/j.ijrmm.2004.08.003.
- Van Voorhis, G.D., Nelson, P.H. & Drake, T.L., 1973. Complex resistivity spectra of porphyry copper mineralization, *Geophysics*, **38**(1), 49–60, doi:10.1190/1.1440333.
- Vanhala, H., 1997a. Laboratory and field studies of environmental and exploration applications of the Spectral Induced Polarization (SIP) method, *PhD thesis*. University of Technology, Helsinki.
- Vanhala, H., 1997b. Mapping oil-contaminated sand and till with the spectral induced polarization (SIP) method, *Geophys. Prospect*, **45**, 303–326.
- Vinegar, H.J. & Waxman, M.H., 1984. Induced polarization of shaly sands, *Geophysics*, **49**(9), 1267–1287.
- Zimmermann, E., Kemna, A., Berwix, J., Glaas, W., Münch, H.M. & Huisman, J.A., 2008. A high-accuracy impedance spectrometer for measuring sediments with low polarizability, *Meas. Sci. Technol.*, **19**, doi:10.1088/0957-0233/19/10/105603.